Sixth International Symposium on Turbulence and Shear Flow Phenomena
Seoul, Korea, 22-24 June 2009

Turbulent Channels, Pipes and Boundary Layers: Similarities and Differences in Large Scale Motions

N. Hutchins, J. Monty, H. Ng, I. Marusic & M. S. Chong
Department of Mechanical Engineering,
University of Melbourne, VIC, 3010, Australia
nhu@unimelb.edu.au

ABSTRACT

This paper details a preliminary comparison between the energy spectra of streamwise velocity fluctuations in zero-pressure-gradient flat-plate turbulent boundary layers (TBL) and turbulent pipe and channel flows. The unique facilities available at the University of Melbourne enable us to investigate these three flows at matched friction Reynolds numbers Re_τ and matched viscous-scaled hot-wire lengths l^+. Detailed maps of energy spectra (calculated from time-series data) reveal important differences between these two flows, particularly in the very large-scale structures that exist in the log and inner wake regions. It is also noted that differences in the large-scale energy between the three geometries extend all the way to the wall. Hence, the commonly held view that the near-wall region is the same across internal and external flows is not strictly true. In general we would recommend caution when comparing statistics between external and internal turbulent flows, especially with increasing Reynolds number.

INTRODUCTION

Despite obvious differences in the wake regions of the mean velocity profiles, there has been a generally held belief, in the past at least, that wall-bounded turbulence in internal and external geometries behave very similarly in the viscous region and that, to some extent, this similarity extends to the overlap (logaithmic) region. The apparent similarities between inner-scaled mean velocity and turbulence intensity profiles for both geometries would have leant some weight to this view, as would the observed similarity of the near-wall cycle between channel and boundary layer flows. Recently, there has been growing evidence that certain dominant length-scales might be different for pipes and channels than for boundary layers. Early indications of these differences came from measurements of cross correlation coefficients and energy spectra of streamwise velocity fluctuations in the streamwise and spanwise directions. Through analysis of premultiplied spectra ($k_x\phi_{uu}$, where k_x is the streamwise wavenumber, and ϕ_{uu} is the energy spectrum of streamwise velocity fluctuations[1]), Kim & Adrian (1999) have reported lengthscales of up to 14 radii in pipe flows (which they termed very large-scale motions, or VLSM). This is in contrast to peak length-scales of 6δ (where δ is the boundary layer thickness) found from similar measurements in the log region of boundary layers (e.g. Hutchins & Marusic, 2007*a*). Balakumar & Adrian (2007) note similar differences between the largest scales in channels and boundary layers. By comparing the log region peak in $k_y\phi_{uu}$ (where k_y is the spanwise wavenumber) between channel DNS and boundary layer experiments (Tomkins & Adrian, 2003; Abe *et al.*, 2004; Kasagi *et al.*, 2005), Hutchins & Marusic (2007*b*) have noted that the spanwise width of the most energetic large-scale structures in internal geometries are larger than those in boundary layers (by a factor of approximately 1.6). Monty *et al.* (2007) have proven this through an in-depth analysis of experimental channel and pipe correlations (further support was recently provided by Bailey *et al.*, 2008).

In general, there is a recently emergent view that the largest-scale motions (and thus the energy spectra) are different for internal and external geometries. This study sets out to analyse, through carefully obtained experimental data, the differences and similarities between the energy spectra for pipes, channels and boundary layers. In order to separate differences due to geometry, from those due to variations in spatial resolution or Reynolds number, an approximately fixed viscous-scaled probe size and friction Reynolds number will be maintained throughout this study.

FACILITY

The channel has a working section of approximately $22 \times 1.17 \times 0.1$ m (channel half-height $h = 0.05$ m). The pipe has a length of 39 m and a radius $r = 0.0494$ m. In both cases, measurements are made at the same development length (175 channel full-heights/pipe diameters downstream of the tripped inlet to the working section). The working Reynolds number range for the channel and pipe facilities is $1000 \lesssim Re_\tau \lesssim 4000$. See Monty *et al.* (2007) for details of these facilities. The High Reynolds Number Boundary Layer Wind Tunnel (HRNBLWT) is an open-return blower wind-tunnel with working section $27 \times 2 \times 1$ m. The nominal Reynolds number range for this facility is $1000 \lesssim Re_\tau \lesssim 25\,000$ (see Hutchins *et al.*, 2009, for full details of the HRNBLWT). A matched target Kármán number of approximately $Re_\tau = 3000$ was selected for comparison, which resulted in the flow conditions presented in table 1. The outer length-scale is here represented by δ_o, which is the boundary layer thickness δ for the TBL (as determined from a modified Coles fit, see Perry *et al.*, 2002), the channel half-height h for channels, and the pipe radius r for pipes.

[1] Throughout this paper, x, y and z will be used to denote the streamwise, spanwise and wall-normal axes, with u, v and w denoting the respective fluctuating velocity components. Lowercase velocities (e.g. u) indicate the fluctuating component. Capitalised velocities (e.g. U) or overbars (e.g. $\overline{u} = 0$) indicate time-averaged values. The superscript $^+$ is used to denote viscous scaling of length (e.g. $z^+ = zU_\tau/\nu$), velocity ($U^+ = U/U_\tau$) and time ($t^+ = tU_\tau^2/\nu$), where U_τ is the friction velocity and ν is the kinematic viscosity.

Facility	Symbol	Flow conditions				
		Re_τ	x (m)	U_∞ (ms^{-1})	δ_o (m)	ν/U_τ (μm)
TBL	☆ —	3020	5.0	12.5	0.10	33.2
Channel	□ – –	3015	17.6	23.1	0.05	16.7
Pipe	○ – ·	3005	17.3	24.3	0.05	16.4

Table 1: Flow parameters for each facility.

Facility	Hot-wire details				Acquisition details		
	l (mm)	d (μm)	l^+	l/d	Δt_s^+	f_s (kHz)	$\frac{TU_\infty}{\delta_o} \times 10^4$
TBL	1	5.0	30	200	0.57	24	2.25
Channel	0.5	2.5	30	200	0.55	100	2.77
Pipe	0.5	2.5	30	200	0.56	100	2.95

Table 2: Hot-wire anemometry and acquisition details.

The friction velocity U_τ is calculated from the pressure drop for the pipe and channel experiments, and from a Clauser fit to mean velocity data for the boundary layer experiments (see figure 1a) using $\kappa = 0.41$ and $A = 5.0$. .

EXPERIMENTS

Boundary layer traverses were conducted in all three facilities at matched friction Reynolds numbers ($Re_\tau = \delta_o U_\tau/\nu$) and matched viscous-scaled wire length ($l^+ = lU_\tau/\nu$). All measurements were made using single-normal hot-wire probes with sensor length l and diameter d. Table 2 gives further anemometry and acquisition details of the matched experiments. Note that in order to keep l^+ and the length-to-diameter ratio (l/d) constant across the three facilities, it was necessary to use smaller diameter wires for the internal geometries. In addition, faster sampling frequencies were required to maintain a constant viscous-scaled sample interval (Δt^+) for the internal geometries. In general, with matched Re_τ the pipe and channel flow facilities will contain higher frequency information than the boundary layer. For example $f^+ = 1/3$ (which Hutchins *et al.*, 2009, suggest as a maximum flow frequency) will equate to frequencies of approximately 5kHz for the TBL, as opposed to 18kHz for the pipe and channel. Hence, for this set of experiments, the internal geometry measurements place more onus on the high-frequency performance of the anemometry. For the channel and pipe experiments, we used an in-house anemometer with a proven frequency response of 50kHz (as determined from impulsive heating of the sensor element using an Nd:YAG laser).

MEAN STATISTICS

Figure 1 shows mean statistics for the three matched facilities. Friction Reynolds number, or Kármán number, is defined as the ratio of an outer length scale (here called δ_o) to the viscous length-scale (ν/U_τ). In attempting to match this ratio across the three facilities, we are faced with the need to define a suitable outer length-scale δ_o. As a first approximation (and following the previous literature) we have assumed that the outer length-scale would be the boundary layer thickness δ (for the TBL) and the channel half-height h and the pipe radius r for the internal geometries. Later, the implications of this choice of length-scale will be addressed. However, for the time being, a cursory inspection of figure 1, would imply that matching Re_τ based on these criteria

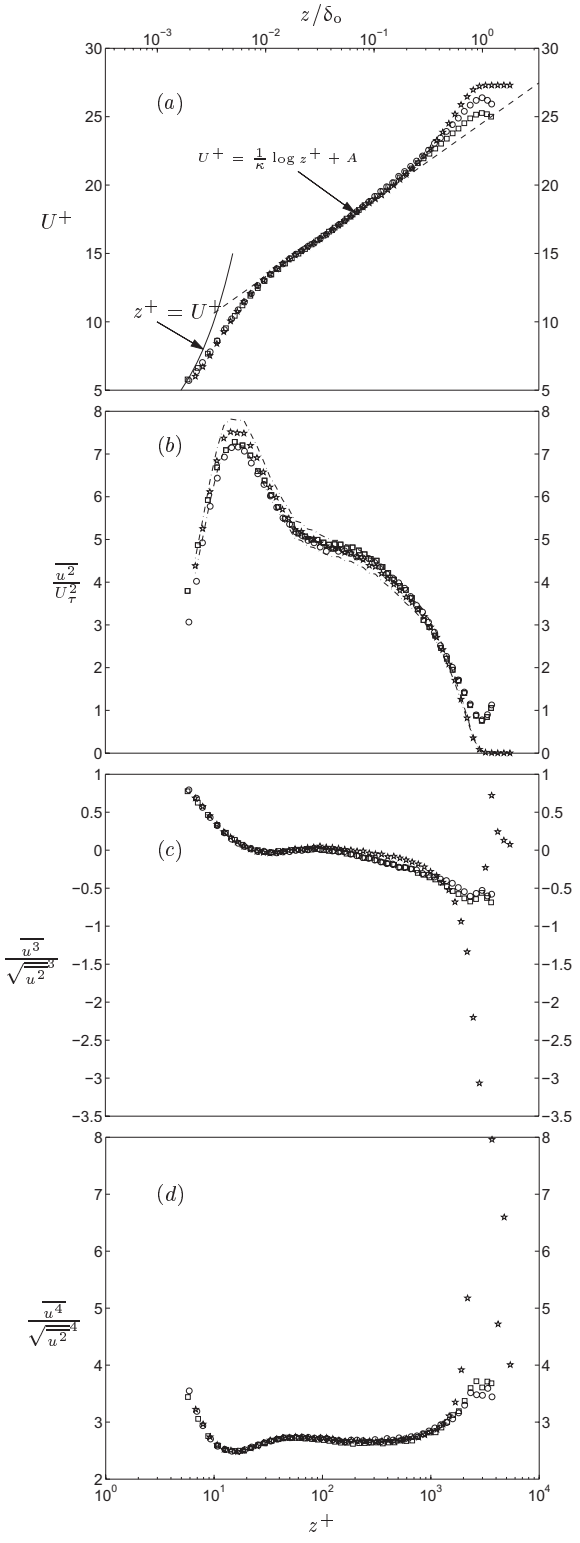

Figure 1: (a) Mean velocity profiles and; (b) associated broadband turbulence intensity; (c) skewness; (d) kurtosis for (□) channel, (○) pipe and (☆) turbulent boundary layer at matched Re_τ. Solid line on (a) shows $U^+ = z^+$. Dashed line shows $U^+ = \frac{1}{\kappa}\ln(z^+) + A$ (where $\kappa = 0.41$ and $A = 5.0$). Dot-dashed lines on (b) shows $\pm 4\%$ variation from TBL data.

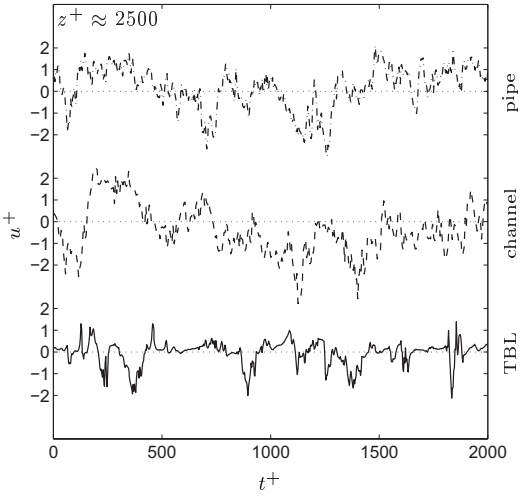

Figure 2: Fluctuating velocity signals at the position of minumum skewness and maximum kurtosis ($z^+ \approx 2500$) for (top to bottom), the ($-\cdot$) pipe; ($--$) channel and (—) TBL.

(and fixed l^+) has done a reasonable job of matching the mean statistics, up to the 4th order, across the external and internal flows. The mean velocity profiles of figure 1(a) exhibit collapse up to the edge of the log region ($z/\delta_o \approx 0.15$, $z^+ \approx 450$), after which the varying wake-strength becomes obvious, with the TBL the strongest, followed by the pipe, and the channel exhibiting the weakest wake-deficit. The collapse in the turbulent intensities of figure 1(b) appears to extend beyond the edge of the log region, to approximately $z/\delta_o = 0.25$ or $z^+ = 1000$ (within the $\pm 4\%$ error bands shown by the dot-dashed lines). Figures 1(c) and (d) show the higher order statistics, skewness and kurtosis. Though the kurtosis exhibits good collapse to beyond $z/\delta_o = 0.25$, it is noted that for the skewness (plot c), the internal geometries exhibit a different trend in the region $100 \lesssim z^+ \lesssim 1000$. Skewness is a measure of asymmetry in the probability distribution of a fluctuating signal. However, recent studies also show that skewness is strongly related to the phase relationship between large- and small-scale fluctuations. It is likely that these differences in skewness will also manifest as differences in the 'amplitude modulation' effect (between large- and small-scales) as studied in Hutchins & Marusic (2007a) and Mathis *et al.* (2009). Beyond $z/\delta_o = 0.5$, Figures 1(c & d) show strong deviations between the higher-order TBL statistics and those for the internal geometries. To explain this difference, figure 2 shows example fluctuating velocity signals from this region of the flow. Clearly the differences in higher order statistics are due to the intermittency that occurs in the outer wake region of the flat-plate boundary layer. For the TBL (the bottom signal on figure 2), patches of predominantly negative small-scale turbulence are interspersed within prolonged periods of relative quiescence, leading to a highly asymmetric and intermittent signal (high skewness and kurtosis). This is in contrast to the internal geometries which both have fully turbulent cores.

PRE-MULTIPLIED ENERGY SPECTRA

Figure 3 shows energy maps of pre-multiplied streamwise energy spectra for all wall-normal positions across the shear layers. The construction of these plots is introduced in some detail in Hutchins & Marusic (2007a,b). Such plots are useful since they show the magnitude of the fluctuating u energy (height of contours) at each wavelength λ_x (y-axis) and for each position z from the wall (x-axis). The top set of contours show the pre-multiplied energy map for the TBL, with a shape and form very similar to that observed previously Hutchins & Marusic (2007a,b). For TBL, such energy maps exhibit two pronounced peaks: termed an 'inner' and 'outer' peak. The inner peak, located at $z^+ \approx 15$ and $\lambda_x^+ \approx 1000$, corresponds to the near-wall cycle of elongated streaks and quasi-streamwise vortices, and is marked in figure 3 by the white '+' symbols. The outer peak is associated with the largest-scale motions that inhabit the log region (termed 'superstructures' in TBL by Hutchins & Marusic, 2007b). It was originally proposed by Hutchins & Marusic (2007b,a) that the outer peak is fixed in outer coordinates at $z/\delta \approx 0.06$ and $\lambda_x/\delta \approx 6$. However, through careful analysis of recent data from Hutchins *et al.* (2009), Mathis *et al.* (2009) have recently shown that this outer peak seems to follow the geometric mid point (in logarithmic axis) of the log region. Assuming the approximate limits for logarithmic behaviour $100 < z^+ < 0.15\delta_o^+$, the midpoint of the log layer, and hence the outer peak, will be located at $z^+ \approx \sqrt{15 Re_\tau}$. This location is marked by the black + symbol on figure 3.

Figures 3(c) & (e) show the corresponding energy maps for the channel and pipe. On initial inspection, all three energy maps (for internal and external flows) exhibit a qualitative similarity, in agreement with Balakumar & Adrian (2007). Indeed, close to the wall, the three energy distributions seem very similar, with a pronounced near-wall maxima well described by the previously defined 'inner peak' location ($z^+ = 15$, $\lambda_x^+ = 1000$). However, closer inspection, reveals an important deviation between the internal and external contours occurring in the log region of the flows (the log region is approximately located in the range $100 \lesssim z^+ \lesssim 450$ at this Re_τ). This difference becomes most obvious in the right-hand-side plots of figure 3 (plots b, d and f) which are plotted with a linear abscissa, highlighting the log and wake regions of the flow. For the TBL, the most energetic length-scales (which peak at $\lambda_x = 6\delta_o$) reduce in wavelength when z^+ is increased beyond $\sqrt{15 Re_\tau}$. By $z^+ = 500$ the most energetic length-scale is reduced to $\lambda_x/\delta_o \approx 3$. For the channel and pipe however, the peak energy continues to move to increasing λ_x/δ_o with increasing z right to the edge of the log region. Indeed, at $z^+ = 500$, the peak energetic length-scale is approximately $\lambda_x = 10\delta_o$, and continues increasing into the wake region. This very large-scale energy in the internal geometries forms a ridge in the contour map (most clear in the linear plots of figure 3d & f). This ridge seems to follow an approximate trend,

$$\lambda_x/\delta_o = C(z/\delta_o)^D \qquad (1)$$

where C is approximately 23 and D is (3/7). This trend is marked by the dashed lines on figure 3(d) & (f). Kim & Adrian (1999) and Balakumar & Adrian (2007) previously found that the energy in the log and core regions of pipe and channel flow exhibits two modes that they term Large-Scale Motion (LSM $\sim 3\delta_o$) and Very Large-Scale Motions (VLSM, which can attain length-scales up to $\sim 14-20\delta_o$). The ridge marked by the dashed line on figure 3d & f is the energetic signature due to the VLSM, and the trend described by eq (1) very closely tracks the evolution of the VLSM as plotted in (Balakumar & Adrian, 2007, figure 2f, p.673). Figure 4 shows the individual pre-multiplied spectra at $z^+ = 500$ for all three flows. In this plot, it is clear that the peak TBL energy occurs around $\lambda_x = 3\delta_o$, whilst the pipe and channel spectra both peak at much longer VLSM wavelengths, as

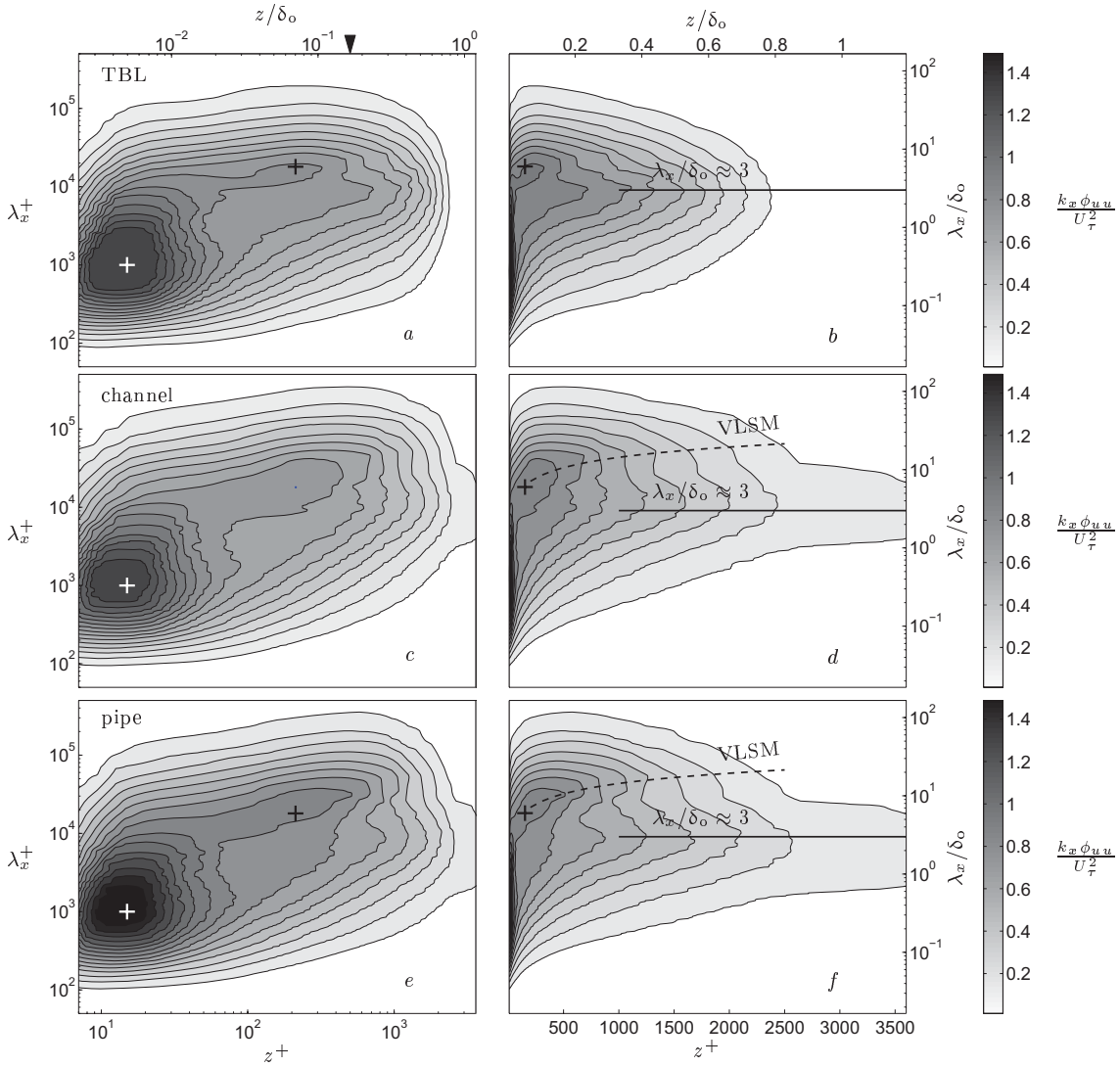

Figure 3: Maps of premultiplied energy spectra of streamwise velocity fluctuation as a function of energetic length-scale (λ_x) and distance from the wall (z). Figures show (from top to bottom) turbulent boundary layer (a,b), channel (c,d) and pipe (e,f) respectively. Left-hand figures have a logarithmic z axis. Right-hand figures (b,d,f) have a linear x-axis.

described by eq. (1). At $z^+ = 500$, the VLSM scale is absent from the turbulent boundary layer spectra shown in figure 4 (the large-scale $6\delta_o$ peak energy is constrained to the log region for the TBL, see figure 3a & b). The differences between the three flows shown in figure 4 are all the more surprising given that the total broadband intensity at this wall-normal location (shown in figure 1b) is almost the same between geometries (and indeed remains so to $z^+ \approx 2000$). Thus the area under the curves shown in figure 4,

$$\int_0^\infty k_x\phi_{uu}\, d(\log \lambda_x) \qquad (2)$$

will be equal for pipes, channel and TBLs. This might suggest that the additional internal geometry constraint on turbulent channel and pipe flows somehow effects a *redistribution* of log and wake region energy into larger scales. Figure 5 shows the energy map for the TBL (figure 3b) subtracted from the energy map for the pipe (figure 3f). This shows the overall difference in premultiplied spectra between the two geometries as a function of λ and z,

$$\Delta k_x\phi_{uu} = |k_x\phi_{uu}(z,\lambda_x)|_{\text{pipe}} - |k_x\phi_{uu}(z,\lambda_x)|_{\text{TBL}}. \qquad (3)$$

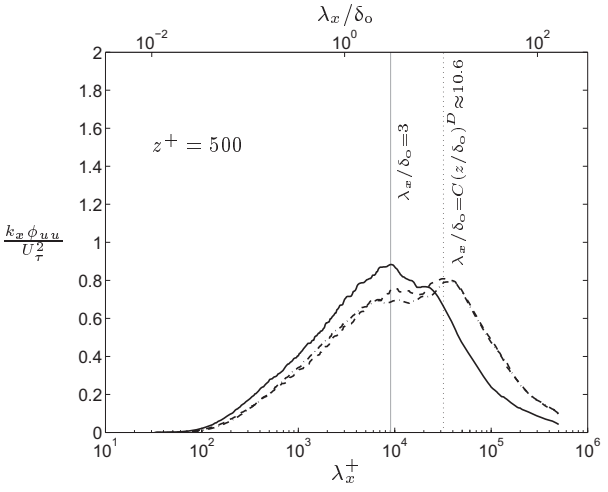

Figure 4: Pre-multiplied energy spectra of u fluctuations for (– ·) pipe; (– –) channel and (—) boundary layer at $z^+ = 500$ (close to the edge of the log region).

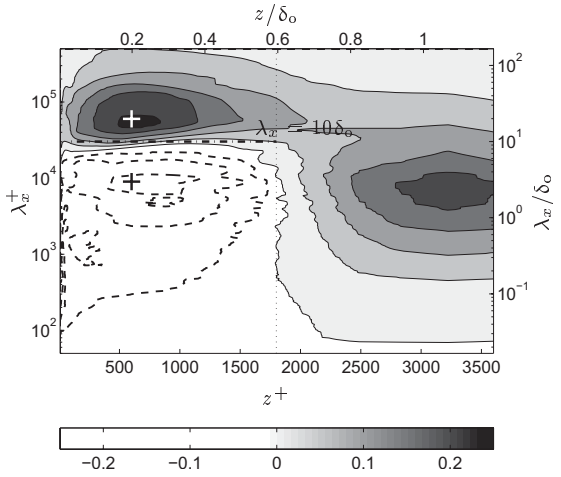

Figure 5: Contours of the difference between the energy spectra ($\Delta k_x \phi_{uu}$) of the pipe and boundary layer as a function of z and λ_x ($|k_x \phi^+_{uu}(z,\lambda_x)|_{\text{pipe}} - |k_x \phi^+_{uu}(z,\lambda_x)|_{\text{TBL}}$). Shaded contours show $\Delta k_x \phi_{uu} > 0$, dashed show < 0.

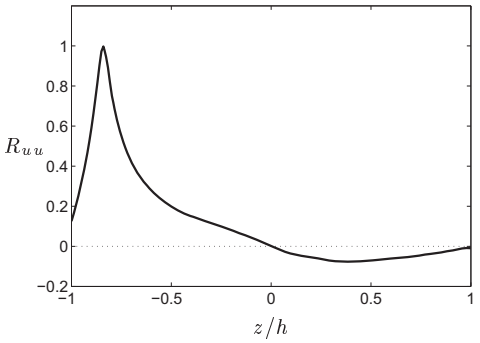

Figure 6: Two-point correlation coefficient of streamwise velocity fluctuations at $z/\delta \approx 0.15$ with the streamwise veloicty across the entire channel height (R_{uu}).

The shaded contours show positive $\Delta k_x \phi_{uu}$, i.e. regions where the pipe has more energy than the TBL. The dashed contours show negative $\Delta k_x \phi_{uu}$ (regions in the map where the TBL has more energy)[2]. Overall there are two clear demarcations in this difference map. The horizontal dot-dashed line on figure 5 shows $\lambda_x = 10\delta_o$. Above this line, the shaded contours indicate that the pipe has additional energy in length-scales greater than $10\delta_o$ as compared to the TBL (and less energy for length-scales less than $10\delta_o$). The peak absolute difference (the location of the maxima and minima above and below $\lambda_x = 10\delta_o$) occurs at $z/\delta_o \approx 0.2$ and $\lambda_x/\delta_o \approx 20$ and 3 respectively, marked by the '+' symbols in figure 5. Remember, that at the wall-normal distance corresponding to these peak differences in energy, figure 1*b* would indicate that the mean broadband intensity is the same for all geometries, supporting the view that the internal geometry constraint causes a redistribution of energy to longer length-scales. In other words, the missing energy in the pipe for $\lambda_x/\delta_o < 10$ is almost perfectly balanced by the additional energy at $\lambda_x/\delta_o > 10$. The second obvious demarcation in figure 5 occurs at $z/\delta_o = 0.6$, shown by the vertical dotted line. To the right of this line (for $z > 0.6\delta$), the pipe has more energy than the TBL at all length-scales due to the turbulent core of the internal geometries. The maximum absolute difference in the core region occurs at $\lambda_x/\delta_o \approx 3$. Figures 3*d* & *e* clearly indicate that the peak energy in the core of the pipe and channel flows occur at these length-scales, which corresponds to the LSM of Kim & Adrian (1999) and Balakumar & Adrian (2007). Finally, it is also noted from figure 5 that the differences in large-scale energy between internal and external geometries extends deep into the near-wall region. Differences in large-scale energy are clearly noticeable at $z^+ = 15$, where geometry effects had previously been assumed to be negligible.

As an additional point, the wavelength λ_x for the energy spectra are calculated from time-series hot-wire data taking the local mean as the convective velocity. In reality, the convection velocity is scale dependent (large-scales will convect faster than small scales). Differences in the distribution of convection velocity could account for some of the variation observed between internal and external geometries.

CHOICE OF OUTER LENGTH-SCALE

In attempting to match the friction Reynolds number across the three facilities, we are forced to make an *a priori* assumption regarding the correct outer length-scale (δ_o) for each geometry. As a first approximation, and for consistency with existing literature, we used the boundary layer thickness for the TBL, and the half-height for the channel and pipe. This is very much the standard definition for each case. This basic assumption appears to do a fairly good job of collapsing the mean and higher order statistics in the logarithmic region. However, in light of the differences in the energy spectra, highlighted in figures 3 - 5 it is prudent to re-evaluate this choice, especially in considering whether the choice of outer length-scale could contribute to the differences observed in the spectra.

There is some suggestion, that δ, h and r may not be the correct choice for the outer length-scale (e.g. Balakumar & Adrian, 2007). For the TBL, the boundary layer thickness at least describes some characteristic length-scale associated with the turbulent flow (approximately representative of the height to which the largest turbulent structures can grow). However, h and r merely indicate the internal half-height of the conduit, and are thus more representative of the mechanical geometry of the facility rather than of any intrinsic length-scale associated with the flow. Indeed, it is clear from correlations, and from instantaneous flow realisations from PIV and DNS, that instantaneous flow structures (or their influence) can extend beyond the centerline in both channels and pipes. As an example of this, figure 6 shows the two-point correlation of u fluctuation across the entire channel, (for a reference point z_{ref} fixed $0.15h$ from the lower wall).

$$R_{uu} = \frac{\overline{u(z_{\text{ref}})u(z)}}{\sigma_u(z_{\text{ref}})\sigma_u(z)}, \qquad (4)$$

$\sigma_u(z)$ is the standard deviation of u at wall-normal location z. This two-point correlation is calculated from a DNS database of turbulent channel flow at $Re_\tau = 934$ (del Álamo *et al.*, 2004), kindly made available by Professor Moser. Though the correlation drops to zero at the channel centerline, the anti-correlated behaviour observed beyond this point, indicates that the structure on the lower half of the channel can influence the behaviour on the upper half (and *vice verse*). Based on this ability for 'crosstalk' in internal flows, one could suggest that the half-height of the conduit

[2]There are only slight differences between the channel and pipe spectra as compared to the TBL (see figure 4). Due to space constraints, $|k_x \phi^+_{uu}(z,\lambda_x)|_{\text{channel}} - |k_x \phi^+_{uu}(z,\lambda_x)|_{\text{TBL}}$ is not plotted here since it is very similar figure 5

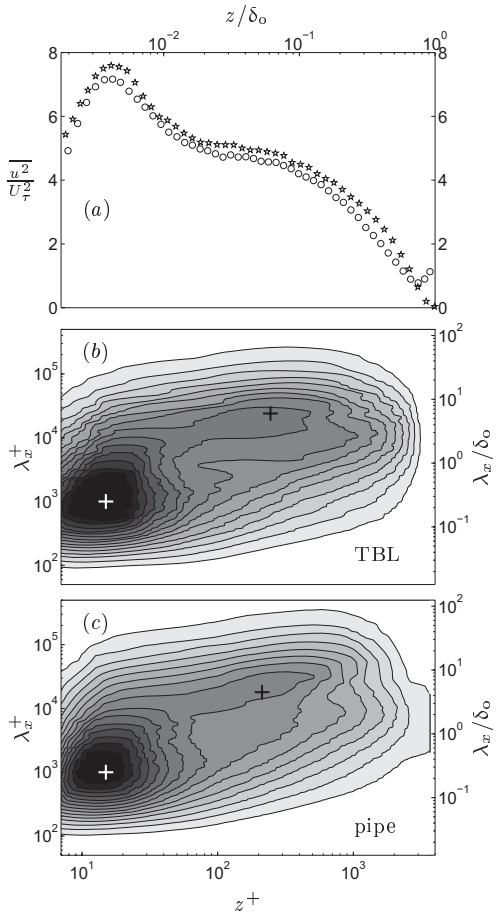

Figure 7: Comparison of TBL and pipe with matched $\delta_o = 1.3r$ ($\delta_o U_\tau/\nu \approx 4000$ and $l^+ \approx 30$). (a) turbulent intensity for (○) pipe and (☆) TBL; and maps of premultiplied energy spectra for (b) TBL; (c) pipe.

may not be the appropriate outer length-scale, and that possibly a larger value should be chosen. In this case the equivalent Re_τ for the channel and the pipe considered here will be greater than the 3000 indicated by assuming the half-height of the conduit as δ_o. To explore whether such an effect could explain the differences observed in the spectra maps, figure 7 compares the same pipe data, with TBL data at $Re_\tau = 4000$ (this would be matched Reynolds number if we assume that $\delta_o = 1.3r$ for the pipe). It is obvious from figure 7(a), that this choice of outer length-scale precludes any collapse in turbulent intensity. By conventional definitions, the TBL data is at a higher Reynolds number than the pipe, and thus the magnitude of the intensity in the log region is higher. Figures 7(b) & (c) indicate that, with this modified outer length-scale, the same differences noted of figure 3 still exist between the energy spectra for the internal and external geometries. Figure 7 reinforces the notion that the spectral surface has a fundamentally different shape for external and internal geometries (the VLSM ridge following $23(z/\delta_o)^{3/7}$ is completely absent from the TBL spectra). No amount of tuning of the outer length-scale can account for the observed differences in the energy spectra between the internal and external geometries.

CONCLUSION

Carefully matched experiments, comparing pipe, channel and TBL have revealed distinct differences in the energy spectra between internal and external flows. The energy surface for the pipe and channel have a different shape than for the TBL. The ridge of energy due to the VLSM (approximately following $23(z/\delta_o)^{3/7}$), noted here in the pipe and channel spectra (and previously by Kim & Adrian, 1999; Balakumar & Adrian, 2007) is absent from the TBL. In general the pipe and channel have more energy than the TBL in length-scales greater than $10\delta_o$. These differences extend down to the near-wall region. Even at $z^+ = 15$, internal geometries exhibit more energy in these large-scales than the TBL. It is shown that alternative choices for the outer length-scale are unlikely to rectify these differences.

The authors gratefully acknowledge the financial support of the Australian Research Council (DP0663499, FF0668703, DP0984577), and the Asian Office of Aerospace Research and Development (AOARD-094023)[3].

REFERENCES

Abe, H., Kawamura, H. & Choi, H. 2004 Very large-scale structures and their effects on the wall shear-stress fluctuations in a turbulent channel flow up to $Re_\tau = 640$. *J. Fluids Eng.* **126**, 835–843.

Bailey, S. C. C., Hultmark, M., Smits, A. J. & Schultz, M. P. 2008 Azimuthal structure of turbulence in high reynolds number pipe flow. *J. Fluid Mech.* **615**, 121–138.

Balakumar, B. J. & Adrian, R. J. 2007 Large- and very-large-scale motions in channel and boundary-layer flows. *Phil. Trans. R. Soc. A* **365**, 665–681.

del Álamo, J. C., Jiménez, J., Zandonade, P. & Moser, R. D. 2004 Scaling of the energy spectra of turbulent channels. *J. Fluid Mech.* **500**, 135–144.

Hutchins, N. & Marusic, I. 2007*a* Evidence of very long meandering features in the logarithmic region of turbulent boundary layers. *J. Fluid Mech.* **579**, 1–28.

Hutchins, N. & Marusic, I. 2007*b* Large-scale influences in near-wall turbulence. *Phil. Trans. R. Soc. A* **365**, 647–664.

Hutchins, N., Nickels, T. B., Marusic, I. & Chong, M. S. 2009 Hot-wire spatial resolution issues in wall-bounded turbulence. *J. Fluid Mech.* Under Review.

Kasagi, K., Fukagata, K. & Suzuki, Y. 2005 Adaptive control of wall-turbulence for skin friction drag reduction and some consideration for high Reynolds number flows. In *2nd Int. Symp. Seawater Drag Reduction*. Busan.

Kim, K. C. & Adrian, R. 1999 Very large-scale motion in the outer layer. *Phys. Fluids* **11**, 417–422.

Mathis, R., Hutchins, N. & Marusic, I. 2009 Large-scale amplitude modulation of the small-scale structures in turbulent boundary layers. *J. Fluid Mech.* In Press.

Monty, J. P., Stewart, J. A., Williams, R. C. & Chong, M. S. 2007 Large-scale features in turbulent pipe and channel flows. *J. Fluid Mech.* **589**, 147–156.

Perry, A. E., Marusic, I. & Jones, M. B. 2002 On the streamwise evolution of turbulent boundary layers in arbitrary pressure gradients. *J. Fluid Mech.* **461**, 61–91.

Tomkins, C. D. & Adrian, R. J. 2003 Spanwise structure and scale growth in turbulent boundary layers. *J. Fluid Mech.* **490**, 37–74.

[3]The views and conclusions contained herein are those of the authors and should not be interpreted as necessarily representing the official policies or endorsements, either expressed or implied, of the Air Force Research Laboratory or the U.S. Government.